Catalysis Today 158 (2010) 29–34

Contents lists available at ScienceDirect

Catalysis Today

journal homepage: www.elsevier.com/locate/cattod

Electrochemical and density functional studies of the catalytic ethylene oxidation on nanostructured Au electrodes

J. Šebera, H. Hoffmannová, P. Krtil*, Z. Samec, S. Záliš*

J. Heyrovský Institute of Physical Chemistry, v.v.i., Academy of Sciences of the Czech Republic, Dolejškova 3, CZ 18223, Prague 8, Czech Republic

ARTICLE INFO

Article history:
Available online 19 June 2010

Keywords:
Electrocatalysis
Ethylene oxidation
DFT
Gold clusters
Nanostructured Au electrodes
Quartz crystal microbalance

ABSTRACT

Electrocatalytic oxidation of ethylene on gold was investigated by means of differential electrochemical mass spectroscopy (DEMS), quartz crystal microbalance (QCM) and DFT calculations. The product analysis indicates a selectivity of the polycrystalline gold towards formation of acetaldehyde. The oxidation process on fresh surface prepared by surface gold oxide reduction, on the other hand, forms mainly carbon dioxide. The oxidation process encompasses metal dissolution. DFT based analysis of the ethylene oxidation on Au clusters was employed to interpret the experimental data. DFT calculations support experimental findings and indicate possible reaction mechanisms of catalytic reactions. DFT calculations point to the different reactivity on individual types of surfaces and different types of clusters.

1. Introduction

The control of the selectivity of the (electro)catalytic processes represents the main challenge in the field of the 21st century. The issue of selectivity is of particular importance in electrode processes involving small organic molecules featuring both single as well as double bonds. In particular oxidative processes connected with oxygen transfer to the molecule like, e.g., oxidation of aliphatic alcohols or insertion of oxygen into double bond [1]. In the latter case there is a need to develop electrocatalytic materials for selective oxygen insertion. One of the possible approaches may be the use gold nanoparticles and clusters which are known to facilitate reactions mechanism unknown on conventional catalysts [2]. In the case of the ethylene oxidation experimental studies indicated the preferential carbon dioxide formation on platinum, the same processes on gold surface yield mixtures of partially oxidized products. In the case of ethylene oxidation on gold the ex situ chromatographic detection found that the oxidation leads to a mixture of aldehydes [3,4]. These studies were later corrected by application of in situ techniques which predicted also formation of CO_2 [5]. As a rule, it is expected that alkenes are oxidized in adsorbed state when both molecules form a flat adsorbate at the electrode via interaction of π electrons of the alkene double bond [5–7].

The fundamental understanding of catalytic reactions at gold nanostructured electrodes is, at present, rather limited. Computational approach to ethylene reactivity providing potential energy curves for different reactant and product conformations may be instrumental in matching the desired mechanism with catalytic surface. The number of theoretical studies (preferably DFT) using cluster approach for modeling the interaction molecules with metal interface has been growing, recently. Calculations have shown the ability to indicate possible pathways for catalytic processes [8–14]. Present work addresses theoretical aspects of the electronic structure of reaction intermediates, ionic distribution at the cluster–solution interface and the more fundamental aspects of looking for transition states in order to map the reaction coordinate of reactions that take place in ethylene oxidation at metal nanoparticles, modeled by Au clusters.

2. Experimental

2.1. Electrochemical experiments

All electrochemical experiments were performed in 0.1 M solution of $HClO_4$ (Flukka, p.a.) in Millipore MilliQ quality de-ionized water. The perchloric acid solutions were saturated with gaseous ethylene (98% Linde) prior to electrochemical experiments. All chemicals were used as received.

The interactions of ethylene with electrode materials were studied by cyclic voltammetry on compact polycrystalline gold disc electrodes with diameter of 4 mm mounted in PTFE holder. The in situ gravimetric experiments were done on a polycrystalline gold forming one of the contacts of a 10 MHz AT-cut quartz crystal (ICMFG OK, USA). The gold substrate was of keyhole shape, sputtered directly on quartz without any under-layer. Piezoac-

* Corresponding authors. Tel.: +420 266053268.
E-mail addresses: petr.krtil@jh-inst.cas.cz (P. Krtil), stanislav.zalis@jh-inst.cas.cz (S. Záliš).

0920-5861/$ – see front matter © 2010 Elsevier B.V. All rights reserved.
doi:10.1016/j.cattod.2010.05.025

tive area of the crystal was 0.22 cm^2. All electrochemical and EQCM experiments were performed in a one-compartment glass cell using three-electrode arrangement with Pt wire auxiliary and saturated calomel reference electrode. The potential control during the experiments was achieved using PAR 263 A potentiostat. The frequency change of the quartz crystal was monitored using in house built EQCM circuitry designed according to that of Bruckenstein [15]. It needs to be noted that the most relevant gold morphology providing relevant data to complement the DFT results should be nanoparticulate gold. On the other hand, the fact that metal nanoparticles are usually stabilized by surface-active species (which can significantly alter the electrocatalytic activity) makes the use of nanoparticulate gold catalysts less convenient.

The analysis of reaction products was performed using the differential electrochemical mass spectroscopy (DEMS). All DEMS experiments were performed on polycrystalline gold sputtered directly on a PTFE membrane (WL Gore) placed in a home-made Kel-F single compartment cell and three electrode arrangement described in [16]. The DEMS apparatus consisted of Prisma™ QMS200 quadrupole mass spectrometer (Balzers) connected to TSU071E turbomolecular drag pumping station (Balzers).

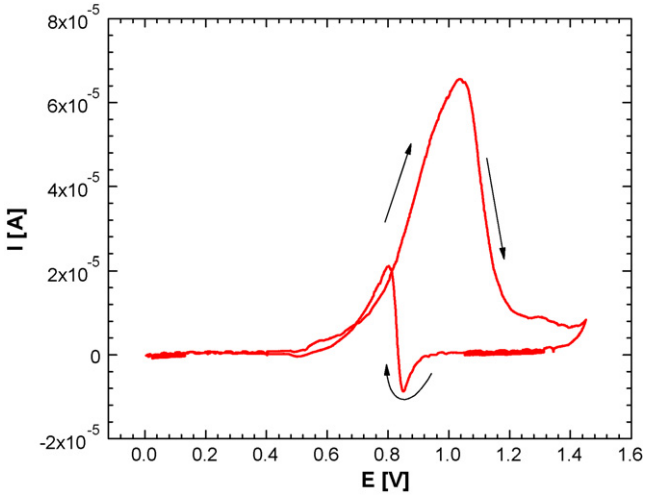

Fig. 1. Cyclic voltammogram of a polycrystalline gold electrode in 0.1 M $HClO_4$ saturated with ethylene at 5 mV/s.

2.2. Computational details

Ground state DFT calculations were performed in Gaussian 03 [17]. Gold clusters were optimized without any geometrical constraint. The calculations were performed for clusters of different structure and size in order to get realistic models of real clusters approximately composing of 100–200 atoms. Optimized ground state geometry of clusters was calculated for the several possible spin multiplicities. Stationary states were characterized by vibrational analysis performed at optimized geometries.

In the present investigation, reaction pathways were investigated by means of hybrid density functional theory with the B3LYP functional [18–20]. The open-shell electronic systems were characterized by unrestricted DFT. The energy profiles of ethylene oxidation presented in this work were obtained using geometrical fixed cluster Au_{22}. Within G03 calculations the quasirelativistic effective core pseudopotentials LANL2DZ (Los Alamos ECP) [21] and the corresponding optimized set of basis functions for Au were used. For H, C and O atoms, 6-31G* [22–23] polarized double ζ basis set was used.

The conductor-like screening model (COSMO) [24] was used for modeling of the solvent influence. External electric field was applied using electric dipole field 0.065 a.u. which modeled the electrochemical potential around 1 V.

3. Results and discussion

3.1. Ethylene oxidation on gold – DEMS approach

Typical cyclic voltammograms of the ethylene oxidation on polycrystalline gold recorded at 5 mV/s is shown in Fig. 1. Ethylene is oxidized in both scans in the potential window between 0.6 V and 1.2 V (vs. SCE). The upper limit of the potential window coincides with the onset of the surface gold oxide formation.

The oxidation of ethylene on Au can be followed by differential electrochemical mass spectroscopy (DEMS). While the DEMS data suggest CO_2 as the only reaction product for the ethylene oxidation on platinum the oxidation on gold proceeds via more complex pathway. The fragments of the consumed ethylene (e.g. $m/z = 27$) decrease in the same potential region where an increase of the anodic current is recorded. The ethylene related signals show gradual recovery at potentials positive to 1.0 V; they do not reach, however, the original values and show further slow decrease at potentials positive to 1.5 V, i.e. in the region where parallel oxygen evolution is observed. The ethylene signal shows very little variance with potential as long as the surface of the electrode is oxide covered. The anodic process following the reduction of surface oxides may be again assigned to ethylene oxidation (see Fig. 2). The signal of ethylene consumption is inversely tracked by signals attributable to fragments of ethylene oxidation products characterized by m/z values of 15, 29, 44 and 43. A fragment with m/z of 32, attributable to molecular oxygen, can be also detected at potentials positive to 1.4 V.

It ought to be noted that the small ethylene concentration decrease at potentials positive to 1.3 V is not inversely tracked by the product mass fragment with m/z of 15, 29 or 43. The only signal which reflects the ethylene consumption in this potential region is the mass fragment with m/z of 44 attributable to formation of carbon dioxide.

The fragments of reaction products are characteristic for either acetaldehyde or oxirane. The formation of the oxirane can be practically ruled out due to weak signal of fragment with the m/z of 15. Relatively strong signal of the fragment with m/z of 44 indicates that the acetaldehyde formation is accompanied with simultaneous carbon dioxide evolution. The selectivity of the polycrystalline gold towards different reaction products seems to be affected (besides of the electrode potential) also by history of the electrode surface. While the fragments attributable to acetaldehyde formation (m/z of 15 and 29) dominate in the potential region between 0.6 V and 1.0 V in the anodic scan, the ethylene consumption in the same potential interval of the cathodic scan (i.e. on the re-activated surface after surface oxide reduction) seems to be accompanied mainly by CO_2 formation. Despite this difference in gold surface selectivity the observed results in principle agree with those reported previously [5].

Since the oxidation of the alkenes on polycrystalline gold may in principle affect the electrode mass, one can use the electrochemical quartz crystal microbalance (EQCM) technique to gather additional information about the studied processes. Although the experimental implementation of EQCM to study the ethylene oxidation is rather straightforward, the analysis of the measured data is complicated by the fact that the anodic polarization of the gold electrode in pure supporting electrolyte solution (0.1 M perchloric acid), i.e. in the absence of dissolved ethylene, is not electrode mass neutral.

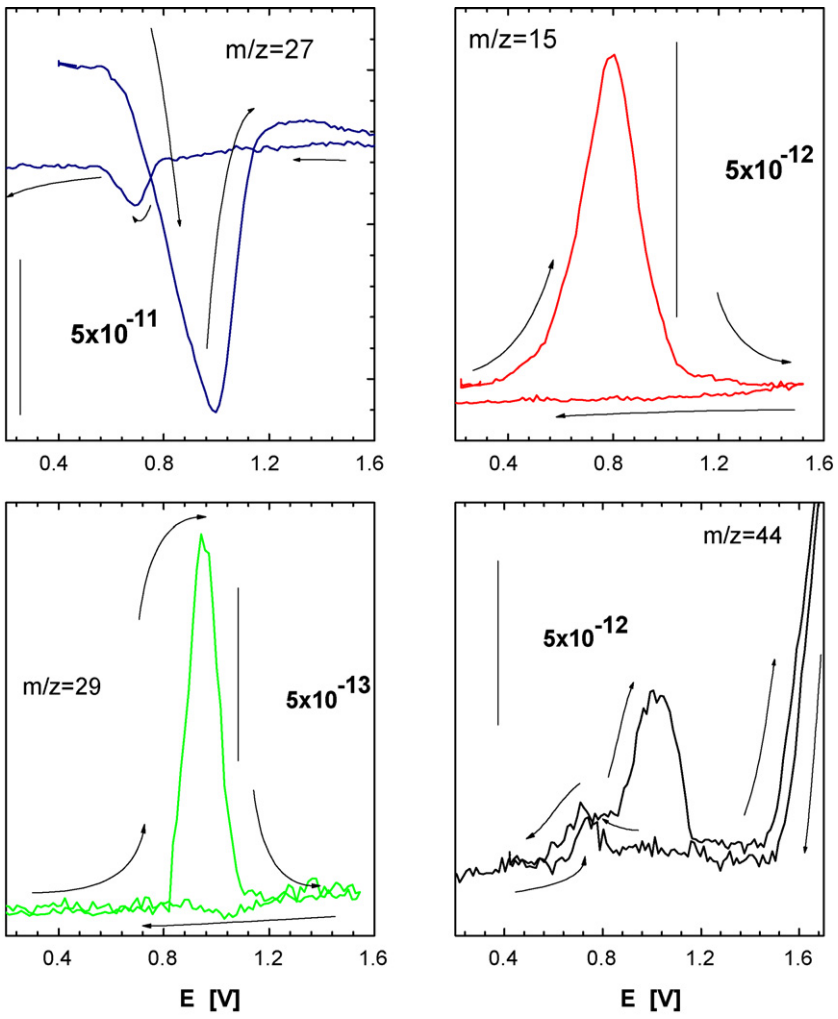

Fig. 2. Potential course of DEMS signals reflecting the abundance of fragments with m/z of 27 (a), 15 (b), 29 (c) and 44 (d) observed during cyclic polarization of a polycrystalline gold electrode in ethylene saturated 0.1 M $HClO_4$ solution at polarization rate of 20 mV/s. The arrows mark the direction of the potential scan.

3.2. Ethylene oxidation on gold – QCM approach

In contrast to the behavior in pure $HClO_4$, the cycling of the polycrystalline gold electrode in perchloric acid solution saturated with ethylene gives time scale dependent Δm vs. E curves. The Δm vs. E curves (see Fig. 3) recorded at scan rates comparable with 50 mV/s are fundamentally the same as those recorded in the absence of ethylene. At slow scan rates ($\nu < 10$ mV/s) the anodic part of the Δm vs. E curve in the potential range between 0.8 V and 1.1 V changes from the plateau (typical for ethylene free behavior) into a mass decrease (see Fig. 3). This electrode mass decrease reverts into weak electrode mass increase at potentials positive to ca. 1.1 V. It needs to be noted that this electrode mass increase is delayed with respect to the electrode mass uptake observed in pure $HClO_4$ solutions. Also the observed electrode mass uptake related to the oxide formation is significantly smaller than that in the case of ethylene free solutions (cf. ca. 3 ng with 15 ng in ethylene absence). The electrode mass remains constant during the initial stage of the cathodic scan until the onset of the surface oxide reduction which is followed by further electrode mass decrease. This behavior indicates that the observed electrode mass change behavior includes relatively slow process(es) of chemical nature which is not controlled by the passed charge. The total electrode mass loss recorded during single cycle increases with decreasing scan rate from ca. 3 ng at 50 mV/s to ca. 40 ng at 5 mV/s. While the electrode mass loss observed at 50 mV/s is generally comparable with that observed in some cases in ethylene free solutions [25] and may be attributed to the instability of the gold due to surface reconstruction, the mass loss recorded at slow scan rate clearly shows the dissolution of gold due to an interaction with ethylene probably as an ethylene–gold complex.

Further information about the ethylene oxidation process can be based on the evaluation of the Δm vs. Q curves constructed from measured data. The typical Δm vs. Q curves constructed from voltammetric data of ethylene oxidation are shown in Fig. 3b. As shown the data in Fig. 3b the electrode mass during the cyclic polarization at first linearly decreases with passed charge. This initial stage of the experiment corresponds to the potential range where the ethylene oxidation is dominant processes at the electrode surface. The slope of Δm vs. Q curve in this region changes with scan rate and gives apparent equivalent mass values between −0.7 g/mol (at 50 mV/s) and −2.6 g/mol (at 5 mV/s). The variability of the observed apparent molar mass indicates that despite the linear response of the measured electrode mass to passed charge the actual character of the mass loss related process is not kinetically controlled by an electrochemical process, but probably by chemical dissolution of surface gold–ethylene complex. The initial linear mass decrease recorded in the region with dominating ethylene oxidation changes into a linear increase (with respect to the passed charge) of the electrode mass. The slope of the rising part of Δm vs. Q curves also shows a dependence on the applied scan rate. The evaluated apparent equivalent mass values range between

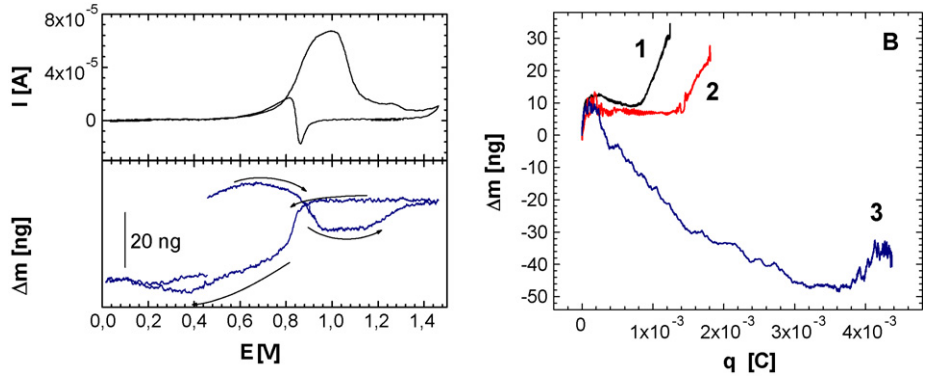

Fig. 3. (A) Cyclic voltammogram and Δm vs. E curve of a polycrystalline gold electrode in ethylene saturated 0.1 M $HClO_4$ solution at scan rate of 5 mV/s. The arrows mark the direction of potential scan. (B) Δm vs Q curves corresponding to cyclic polarization of a polycrystalline gold electrode in ethylene saturated 0.1 M $HClO_4$ solution at scan rate of 50 mV/s (a), 20 mV/s (b) and 5 m/s (c).

5.3 g/mol (at 50 mV/s) and 2.7 g/mol (at 5 mV/s) and are lower than those observed on polycrystalline gold cycled in pure $HClO_4$. The observed trend indicates that the surface oxide formation or more precisely the re-solvation processes connected with its formation is restricted in the presence of ethylene and proceeds only on a fraction of the surface.

3.3. DFT modeling of ethylene oxidation on gold clusters

DFT method was used for the modeling of gold clusters and their interaction with organic molecules. In order to model mechanisms of the ethylene oxidation at Au clusters, the formation of M_x–Et–O intermediates and the possible intermediate transfer under the influence of electric field or electrode reaction was studied. The understanding of catalytic properties of surface requires the proper description of the interface. Prior the study of surface interactions, planar and three-dimensional Au_n clusters up the size of 22 atoms were modeled as an interface simplification or as a part of real experimental systems. Clusters of different size were optimized in the respect to different spin states without constraints. The interaction with the surface depends on the type of the cluster, its size and the reaction site.

The geometry of Au_n clusters was based on Au(1 1 1) structure with spin multiplicity depending on a number of atoms included in the cluster. Two pyramidal $Au_{21}(^2A)$ and $Au_{22}(^1A)$ clusters (see Fig. 4) were optimized by DFT methodology. Averaged interatomic distances of gold atoms in clusters were 2.87 Å {2.76–3.05 Å} within $Au_{21}(^2A)$ and 2.93 Å {2.76–3.24 Å} within $Au_{22}(^1A)$. These distances correspond very well to the experimental value of the Au–Au bulk distance in Au(1 1 1) 2.88 Å [26]. Fig. 4 shows structures of three-dimensional Au_{22} cluster which was chosen in order to describe the

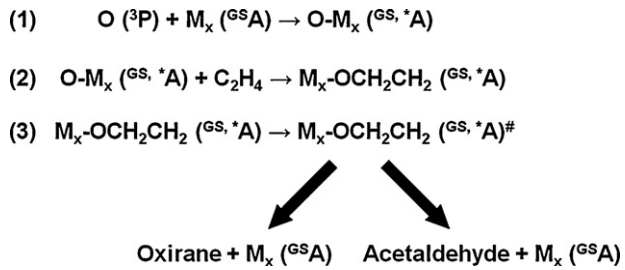

Scheme 1. Pathways used in modeling of ethylene oxidation at M_x clusters. GS, *, and # symbolize ground, activated and transition states, respectively.

plane steps and edges. Optimized structure of cluster $Au_{22}(^1A)$ was used in the following examination of intermediates and transition states in a three-step process of ethylene oxidation by triplet and singlet oxygen according to Scheme 1.

Two possible oxygen interactions within the clusters were considered: plane interaction (oxygen is bonded to the three atoms) and edge interaction (oxygen is bonded to the two atoms). The optimized structures of M_x–O are similar to already published [13,28–30]. In the case of plane interaction, the averaged length of O–Au distances is 2.157 Å (singlet state) and 2.212 Å (triplet state). The edge interaction leads to the averaged distances of Au–O 2.032 Å (singlet state) and 2.183 Å (triplet state). DFT calculated negative reaction energies ΔG_r for interaction between free atomic oxygen (^3A) and both gold clusters as the reactants indicate the formation of stable O–M_x intermediates.

It may be expected that the interaction of the adsorbed oxygen with ethylene leads to the stable surface oxametallacycle intermediates in a process similar to that of ethylene oxide reaction at

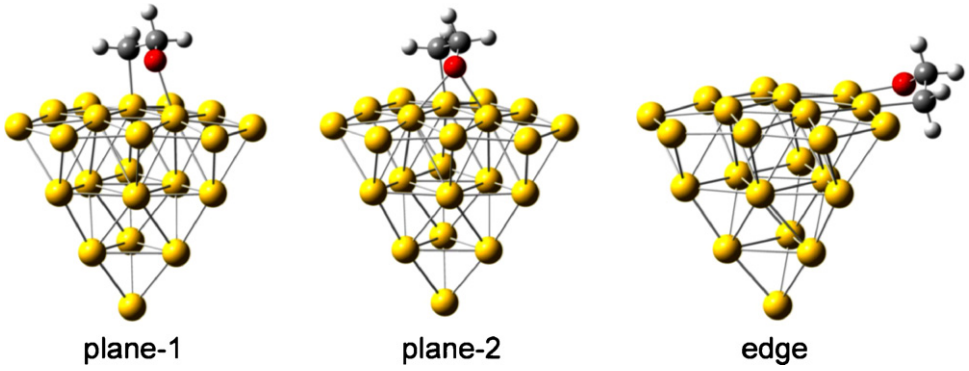

Fig. 4. DFT optimized structures of oxametallacycle intermediates interacting with $Au_{22}(^1A)$ clusters.

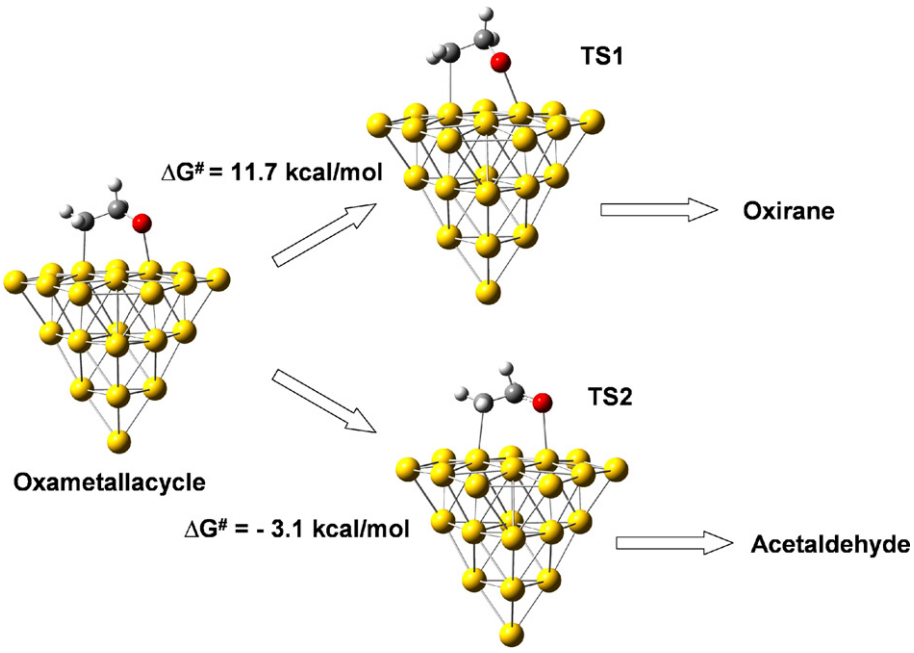

Fig. 5. DFT optimized structure of oxametallacycle intermediate O–CH_2CH_2–Au_{22}(^{1}A) {plane-1} and optimized transition states leading to oxirane and acetaldehyde.

Ag(1 1 1) surface [8–9,31–32]. The geometry of clusters was fixed during the geometry optimization and transition structure search, the remaining part of the system was fully optimized. The interaction with the surface depends on the type of the cluster, its size and multiplicity and the reaction site (the plane steps or edges). Fig. 4 shows the optimized structures of oxametallacycle intermediates formed at Au_{22} cluster characterized by different orientation of $-OCH_2CH_2$ over the surface. Table 1 lists selected DFT calculated bond lengths characterizing oxametallacycle intermediates. Table 2 summarizes the DFT calculated ΔG_r values for reactions between free ethylene and O–Au_{22} clusters leading to oxametallacycle intermediates Au_{22}–OCH_2CH_2. DFT calculated transition state activation energies $\Delta G^{\#}$ and the reaction energies ΔG_r of oxirane or acetaldehyde formation are given in Table 3. DFT optimized structure of transition states leading from oxametallacycle intermediate O–CH_2CH_2–Au_{22}(^{1}A) {plane-1} either to oxirane or acetaldehyde is depicted in Fig. 5. The formation of acetaldehyde for O–CH_2CH_2–Au_{22}(^{1}A) {plane-1} is barrier-less. This clearly favors the formation of acetaldehyde as the main reaction product.

The reaction energetics is only slightly influenced by the static electric field corresponding to the electrochemical potential around 1 V or by the influence of solvent cavity. The large activation barrier for ethylene oxidation in gas phase is slightly lowered by a solvent effect. External effects influence transition states and thermodynamics properties but do not qualitatively change the reaction profiles.

The results of the DFT calculations are in accordance with experimental results of electrocatalytic oxidation of ethylene on gold using DEMS outlined above.

Table 1
Selected DFT calculated bond lengths (Å) for stable Au_{22}–OCH_2CH_2 oxametallacycles.

Au_{22}–OCH_2CH_2(^{1}A) {plane-1}	Length	Au_{22}–OCH_2CH_2(^{3}A) {plane-1}	Length
Au1–O	2.281	Au1–O	2.238
Au2–O	3.017	Au2–O	3.518
Au3–C2	2.242	Au3–C2	2.255
O–C1	1.361	O–C1	1.365
C1–C2	1.503	C1–C2	1.511
Au_{22}–OCH_2CH_2(^{1}A) {plane-2}		Au_{22}–OCH_2CH_2(^{3}A) {plane-2}	
Au1–O	2.352	Au1–O	2.335
Au2–O	2.535	Au2–O	2.468
Au3–C2	2.226	Au3–C2	2.237
O–C1	1.379	O–C1	1.395
C1–C2	1.503	C1–C2	1.512
Au_{22}–OCH_2CH_2(^{1}A) {edge}		Au_{22}–OCH_2CH_2(^{3}A) {edge}	
Au1–O	2.045	Au1–O	2.092
Au2–2	2.157	Au2–C2	2.206
O–C1	1.410	O–C1	1.388
C1–C2	1.523	C1–C2	1.509

Table 2
DFT calculated ΔG_r of the reaction between free ethylene and O–Au_{22} cluster leading to oxametallacycle intermediates Au_{22}–OCH_2CH_2.

Au_{22}–O + C_2H_2 → Au_{22}–OCH_2CH_2	ΔG_r (kcal/mol)
Au_{22}–OCH_2CH_2(^{1}A) {plane-1}	−7.0
Au_{22}–OCH_2CH_2(^{1}A) {plane-2}	−6.4
Au_{22}–OCH_2CH_2(^{1}A) {edge}	−10.8
Au_{22}–OCH_2CH_2(^{3}A) {plane-1}	−8.1
Au_{22}–OCH_2CH_2(^{3}A) {plane-2}	−6.6
Au_{22}–OCH_2CH_2(^{3}A) {edge}	−16.2

Table 3
DFT calculated transition state activation energies $\Delta G^{\#}$ and the reaction energies ΔG_r of oxirane or acetaldehyde formation.

Gold cluster–oxirane product	$\Delta G^{\#}$ (kcal/mol)	ΔG_r (kcal/mol)
Au_{22}–OCH_2CH_2(^{1}A) {plane-1}	11.7	−48.8
Au_{22}–OCH_2CH_2(^{1}A) {plane-2}	11.2	−49.3
Au_{22}–OCH_2CH_2(^{3}A) {edge}	17.5	−25.4
Gold cluster–acetaldehyde product		
Au_{22}–OCH_2CH_2(^{1}A) {plane-1}	−3.1	−78.0
Au_{22}–OCH_2CH_2(^{3}A) {plane-1}	2.9	−81.3
Au_{22}–OCH_2CH_2(^{1}A) {plane-2}	−3.7	−78.6
Au_{22}–OCH_2CH_2(^{3}A) {plane-2}	1.4	−82.8
Au_{22}–OCH_2CH_2(^{1}A) {edge}	15.0	−50.8
Au_{22}–OCH_2CH_2(^{3}A) {edge}	11.0	−54.7

4. Conclusions

The anodic oxidation of ethylene on gold leads to a formation of acetaldehyde as a major product; small fraction of ethylene is oxidized to carbon dioxide in parallel. The selectivity of the gold surface towards different reaction products depends on the electrode history as reflects the selective CO_2 formation of gold surface obtained by reduction of the surface oxide. The ethylene oxidation accompanies notable dissolution of the electrode material. This process is of chemical nature and proceeds on oxide free metal surface. The DFT calculations support experimental findings and indicate possible reaction mechanisms of catalytic reactions. DFT calculations points to the different reactivity on individual types of surfaces and different types of clusters. The adopted theoretical approach, however, cannot address the experimentally observed metal dissolution.

Acknowledgements

This work was supported by European COST action and the Academy of Sciences of the Czech Republic (grant KAN100400702). The computer time at the METACentrum is gratefully acknowledged.

References

[1] S. Otsuka, I. Yamanaka, Catal. Today 41 (1998) 311.
[2] T. Ishida, M. Haruta, Angew. Chem. Int. Ed. 46 (2007) 7154–7156.
[3] J.W. Johnson, S.C. Lai, W.J. James, Electrochim. Acta 15 (1970) 1511.
[4] L. Cwiklinski, J. Perichon, Electrochim. Acta 19 (1974) 297.
[5] E. Pastor, V.M. Schmidt, J. Electroanal. Chem. 383 (1995) 175.
[6] T. Loffler, H. Baltruschat, J. Electroanal. Chem. 554–555 (2003) 333.
[7] U. Muller, U. Schmiemann, A. Dulberg, H. Baltruschat, Surf. Sci. 335 (1995) 333.
[8] S. Linic, M.A. Barteau, J. Am. Chem. Soc. 124 (2002) 310.
[9] S. Linic, M.A. Barteau, J. Catal. 214 (2003) 200–212.
[10] T.V. de Bocarme, T.D. Chau, F. Tielens, J. Andres, P. Gaspard, R.L.C. Wang, H.J. Kreuzer, N. Kruse, J. Chem. Phys. 125 (2006).
[11] B. Yoon, P. Koskinen, B. Huber, O. Kostko, B. von Issendorff, H. Hakkinen, M. Moseler, U. Landman, Chemphyschem. 8 (2007) 157–161.
[12] H.T. Chen, J.G. Chang, S.P. Ju, H.L. Chen, J. Comput. Chem. 31 (2010) 258–265.
[13] Y. Wang, X.G. Gong, J. Chem. Phys. 125 (2006) 124703.
[14] S. Záliš, I. Kratochvilova, A. Zambova, J. Mbindyo, T.E. Mallouk, T.S. Mayer, Eur. Phys. J. E 18 (2005) 201–206.
[15] S. Bruckenstein, M. Michalski, A. Fensore, Z.F. Li, A.R. Hillman, Anal. Chem. 66 (1994) 1847.
[16] R. Imhof, P. Novak, J. Electrochem. Soc. 146 (1999) 1702.
[17] M.J. Frisch, G.W. Trucks, H.B. Schlegel, G.E. Scuseria, M.A. Robb, J.R. Cheeseman, J. Montgomery, T. Vreven, K.N. Kudin, J.C. Burant, J.M. Millam, S.S. Iyengar, J. Tomasi,V. Barone, B. Mennucci, M. Cossi, G. Scalmani, N. Rega, G.A. Petersson, H. Nakatsuji, M. Hada, M. Ehara, K. Toyota, R. Fukuda, J. Hasegawa, M. Ishida, T. Nakajima, Y. Honda, O. Kitao, H. Nakai, M. Klene, X. Li, J.E. Knox, H.P. Hratchian, J.B. Cross, C. Adamo, J. Jaramillo, R. Gomperts, R.E. Stratmann, O. Yazyev, A.J. Austin, R. Cammi, C. Pomelli, J.W. Ochterski, P.Y. Ayala, K. Morokuma, G.A. Voth, P. Salvador, J.J. Dannenberg, V.G. Zakrzewski, S. Dapprich, A.D. Daniels, M.C. Strain, O. Farkas, D.K. Malick, A.D. Rabuck, K. Raghavachari, J.B. Foresman, J.V. Ortiz, Q. Cui, A.G. Baboul, S. Clifford, J. Cioslowski, B.B. Stefanov, G. Liu, A. Liashenko, P. Piskorz, I. Komaromi, R.L. Martin, D.J. Fox, T. Keith, M.A. Al-Laham, C.Y. Peng, A. Nanayakkara, M. Challacombe, P.M.W. Gill, B. Johnson, W. Chen, M.W. Wong, C. Gonzalez, J.A. Pople, Gaussian 03, Revision E.01, Gaussian, Inc., Pittsburg, PA, 2004.
[18] A.D. Becke, J. Chem. Phys. 98 (1993) 5648.
[19] P.J. Stevens, F.J. Devlin, C.F. Chablowski, M.J. Frisch, J. Phys. Chem. 98 (1994) 11623.
[20] C. Lee, W. Yang, R.G. Parr, Phys. Rev. B 37 (1988) 785.
[21] P.J. Hay, W.R. Wadt, J. Chem. Phys. 82 (1985) 299.
[22] M.M. Francl, W.J. Pietro, W.J. Hehre, J.S. Binkley, D.J. DeFrees, J.A. Pople, M.S. Gordon, J. Chem. Phys. 77 (1982) 3654.
[23] V.A. Rassolov, J.A. Pople, M.A. Ratner, T.L. Windus, J. Chem. Phys. 109 (1998) 1223.
[24] A. Klamt, V. Jones, J. Chem. Phys. 105 (1996) 9972.
[25] S. Bruckenstein, M. Shay, J. Electroanal. Chem. 188 (1985) 131.
[26] J. Li, X. Li, H.-J. Zhai, L.-S. Wang, Science 299 (2003) 864.
[28] B. Yoon, H. Hakkinen, U. Landman, J. Phys. Chem. A 107 (2003) 4066.
[29] X. Lin, N.J. Ramer, A.M. Rappe, K.C. Hass, W.F. Schneider, B.L. Trout, J. Phys. Chem. B 105 (2001) 7739.
[30] T. Jacob, R.P. Muller, W.A. Goddard, J. Phys. Chem. B 107 (2003) 9465.
[31] S. Linic, H. Piao, K. Adib, M.A. Barteau, Angew. Chem. Int. Ed. 43 (2004) 2918.
[32] S. Linic, M.A. Barteau, J. Am. Chem. Soc. 125 (2003) 4034–4035.